Available online at www.sciencedirect.com
SCIENCE DIRECT®
International Journal of Multiphase Flow 31 (2005) 1134–1154
International Journal of Multiphase Flow
www.elsevier.com/locate/ijmulflow

Stability of a liquid jet into incompressible gases and liquids: Part 2. Effects of the irrotational viscous pressure

T. Funada [a], M. Saitoh [a], J. Wang [b], D.D. Joseph [b,*]

[a] *Department of Digital Engineering, Numazu College of Technology, Ooka 3600, Numazu, Shizuoka 410-8501, Japan*
[b] *Department of Aerospace Engineering and Mechanics, University of Minnesota, Minneapolis, MN 55455, USA*

Received 8 April 2005; received in revised form 22 June 2005

Abstract

In this paper we investigate the effects of an irrotational, viscous pressure on the stability of a liquid jet into gases and liquids. The analysis extends our earlier work (part 1) in which the stability of the viscous jet was studied assuming that the motion and pressure are irrotational and the viscosity enters through the jump in the viscous normal stress in the normal stress balance at the interface. The liquid jet is always unstable; at high Weber numbers the instability is dominated by capillary instability; at low W the instability is dominated by Kelvin–Helmholtz (KH) waves generated by pressures driven by the discontinuous velocity. In the irrotational analysis the viscosity is important but the effects of shear are neglected. In fact a discontinuous velocity is not compatible with the continuity of the tangential components of velocity and shear stress so that KH instability is not properly posed for exact study using the no-slip condition but some of the effects of viscosity can be ascertained using viscous potential flow. The theory is called viscous potential flow (VPF). Here we develop another irrotational theory in which the discontinuities in the irrotational tangential velocity and shear stress are eliminated in the global energy balance by selecting viscous contributions to the irrotational pressure. These pressures generate a hierarchy of potential flows in powers of the viscosity, but only the first one, linear in viscosity, in the irrotational viscous stress, is thought to have physical significance. The tangential velocity and shear stress in an irrotational study cannot be made continuous, but the effects of the discontinuous velocity and stress in the mechanical energy balance can be

* Corresponding author. Tel.: +1 612 626 8000; fax: +1 612 626 1558.
E-mail address: joseph@aem.umn.edu (D.D. Joseph).

0301-9322/$ - see front matter
doi:10.1016/j.ijmultiphaseflow.2005.06.007

removed "in the mean." This theory with the additional viscous pressure is called VCVPF, viscous correction of VPF. VCVPF is VPF with the additional pressures. The theory here cannot be compared with an exact solution, which would not allow the discontinuous velocity and stress. In other problems, like capillary instability, in which VCVPF can be compared with an exact solution, the agreements are uniformly excellent in the wave number when one of the fluids is gas and in good but not uniform, agreement when both fluids are liquids.

Keywords: VCVPF (Viscous correction of viscous potential flow); Kelvin–Helmholtz (KH) instability; Capillary instability

1. Introduction

This note is an addendum to the paper "Stability of a Liquid Jet into Incompressible Gases and Liquids" by Funada et al. (2004). The analysis in that paper is based on viscous potential flow; the viscosity enters through the viscous term in the normal stress balance and only there. Another way to use the potential flow to study problems of stability of viscous fluids is through the dissipation method; the two theories are not the same. The dissipation method is based on an evaluation of the equation governing the evolution of the energy on fields $u = \nabla\phi$ where $\nabla^2\phi = 0$, and only these. The viscosity enters as the coefficient of the dissipation integral and in the evaluation of certain viscous stress at the boundary. This method has been applied by Lamb (1932) to compute the decay of water waves due to viscosity, by Levich (1949) to compute the drag on a spherical gas bubble, by Wang et al. (2005a) to study capillary instability of a liquid cylinder in gas or vacuum and by Wang et al. (2005b) to study the capillary instability of two fluids, or even two liquids. When the outside fluid is gas or vacuum, the two fluid formulation gives outstanding results; the growth rate curves are at most a few percent different than those computed from the exact normal mode theory in which nonslip conditions are satisfied and the velocity fields are rotational. In the case of the stability of a liquid jet considered here, we must carry out the analysis with a two-fluid theory. It was shown by Funada et al. (2004) that the jet is unstable to capillary instabilities when the Weber number W is very large and Kelvin–Helmholtz waves when the Weber number is very small. Though capillary instability can occur in vacuum, KH instability cannot; an outside fluid is required.

The relation between the dissipation method and viscous potential flow (VPF) is of interest. It was shown by Joseph and Wang (2004) that the two theories could give rise to identical results if an additional normal stress in the form of a viscous correction of the irrotational pressure was computed from an algorithm based on the notion that this extra contribution is induced in a thin boundary layer, not computed and not needed, by the uncompensated irrotational shear stresses in the precise way indicated by equation (2.5). The theory of the added pressure, which leads to the same results as the dissipation method is called VCVPF (viscous correction of viscous potential flow). VCVPF is VPF with the added pressure. In this paper we work out VCVPF for the stability problem studied using VPF by Funada et al. (2004).

2. Problem formulation

A long liquid cylinder of density ρ, viscosity μ, and of mean radius a moves with a uniform axial velocity U relative to an ambient gas (air) of ρ_a, μ_a. With a cylindrical frame (r,θ,z) fixed on the gas, the liquid cylinder is put in the region of $0 \leqslant r < a+\eta$ and $-\infty < z < \infty$, where $\eta = \eta(\theta,z,t)$ is the interface displacement.

A hierarchy of potential flows may be defined; IFF stands for the potential flow of an inviscid fluid, VPF stands for the potential flow of a viscous fluid in which the viscosity enters through the viscous normal stress and is otherwise identical to IPF. VCVPF is a viscous correction to VPF, which is the same as VPF except that pressure contributions are introduced to remove the effects of the irrotational tangential velocities and stress in the energy equations.

The mechanical energy equations for the outside and inside fluids are respectively

$$\begin{aligned}\frac{\mathrm{d}}{\mathrm{d}t}\int_{V_a}\frac{\rho_a}{2}|\boldsymbol{u}_a|^2\,\mathrm{d}V &= \int_{\Omega}[\boldsymbol{u}_a\cdot\mathbf{T}_a\cdot\boldsymbol{n}_2]\,\mathrm{d}\Omega - \int_{V_a}2\mu_a\mathbf{D}_a:\mathbf{D}_a\,\mathrm{d}V\\ &= -\int_{\Omega}[\boldsymbol{u}_a\cdot\boldsymbol{n}_1(-p_a+\tau_a^n)+\boldsymbol{u}_a\cdot\boldsymbol{t}\tau_a^s]\,\mathrm{d}\Omega - \int_{Va}2\mu_a\mathbf{D}_a:\mathbf{D}_a\,\mathrm{d}V, \qquad (2.1)\\ \frac{\mathrm{d}}{\mathrm{d}t}\int_{V_l}\frac{\rho_l}{2}|\boldsymbol{u}_l|^2\,\mathrm{d}V &= \int_{\Omega}[\boldsymbol{u}_l\cdot\mathbf{T}_l\cdot\boldsymbol{n}_1]\,\mathrm{d}\Omega - \int_{V_l}2\mu_l\mathbf{D}_l:\mathbf{D}_l\,\mathrm{d}V\\ &= \int_{\Omega}[\boldsymbol{u}_l\cdot\boldsymbol{n}_1(-p_l+\tau_l^n)+\boldsymbol{u}_l\cdot\boldsymbol{t}\tau_l^s]\,\mathrm{d}\Omega - \int_{V_l}2\mu_l\mathbf{D}_l:\mathbf{D}_l\,\mathrm{d}V, \qquad (2.2)\end{aligned}$$

where $\boldsymbol{n}_1 = -\boldsymbol{n}_2$ is the outward normal vector to the surface Ω.

With the continuity of the normal velocity

$$\boldsymbol{u}_a\cdot\boldsymbol{n}_1 = \boldsymbol{u}_l\cdot\boldsymbol{n}_1 = u_n, \qquad (2.3)$$

the sum of (2.1) and (2.2) can be written as

$$\begin{aligned}\frac{\mathrm{d}}{\mathrm{d}t}\int_{V_a}\frac{\rho_a}{2}|\boldsymbol{u}_a|^2\,\mathrm{d}V + \frac{\mathrm{d}}{\mathrm{d}t}\int_{Vl}\frac{\rho_l}{2}|\boldsymbol{u}_l|^2\,\mathrm{d}V &= \int_{\Omega}[u_n(-p_l+\tau_l^n+p_a-\tau_a^n)+\boldsymbol{u}_l\cdot\boldsymbol{t}\tau_l^s-\boldsymbol{u}_a\cdot\boldsymbol{t}\tau_a^s]\,\mathrm{d}\Omega\\ &\quad - \int_{V_a}2\mu_a\mathbf{D}_a:\mathbf{D}_a\,\mathrm{d}V - \int_{V_l}2\mu_l\mathbf{D}_l:\mathbf{D}_l\,\mathrm{d}V. \qquad (2.4)\end{aligned}$$

To obtain a purely irrotational theory for the stability of the jet, we evaluate (2.3) and (2.4) on $\boldsymbol{u} = \nabla\phi$. The shear stress and tangential component of velocity cannot be made continuous at $r = a+\eta$ but these conditions can be satisfied "in the mean" by the introduction of two pressure corrections p_l^v and p_a^v such that

$$p_l = p_l^i + p_l^v, \quad p_a = p_a^i + p_a^v,$$

where p^i is the pressure given by Bernoulli equation (the same pressure you get from potential flow of an inviscid fluid). Hence

$$\int_{\Omega}u_n(-p_l^v+p_a^v)\,\mathrm{d}\Omega = \int_{\Omega}(\boldsymbol{u}_l\cdot\boldsymbol{t}\tau_l^s-\boldsymbol{u}_a\cdot\boldsymbol{t}\tau_a^s)\,\mathrm{d}\Omega. \qquad (2.5)$$

Joseph and Wang (2004) showed that in linearized problems, the governing equation for the pressure corrections is

$$\nabla^2 p^v = 0. \tag{2.6}$$

Eqs. (2.5) and (2.6) can be satisfied uniquely, as we show in the next section. For now, it will suffice to note that p_l^v, p_a^v are proportional to μ_l and μ_a and

$$\rho_l\left(\frac{\partial \boldsymbol{u}_l^v}{\partial t} + U\frac{\partial \boldsymbol{u}_l^v}{\partial z}\right) = \mu_l \nabla^2 \boldsymbol{u}_l^v - \nabla p_l^v, \tag{2.7}$$

$$\rho_a \frac{\partial \boldsymbol{u}_a^v}{\partial t} = \mu_a \nabla^2 \boldsymbol{u}_a^v - \nabla p_a^v. \tag{2.8}$$

We can find potential flow solutions of (2.7) and (2.8), $\nabla^2\phi^v = \nabla^2\phi_a^v = 0$, such that

$$\boldsymbol{u}_l^v = \nabla\phi^v, \quad \boldsymbol{u}_a^v = \nabla\phi_a^v, \tag{2.9}$$

where

$$\rho_l\left(\frac{\partial \phi^v}{\partial t} + U\frac{\partial \phi^v}{\partial z}\right) = -p_l^v, \tag{2.10}$$

$$\rho_a \frac{\partial \phi_a^v}{\partial t} = -p_a^v \tag{2.11}$$

and

$$\frac{\partial \phi^v}{\partial r} - U\frac{\partial \eta^v}{\partial z} = \frac{\partial \phi_a^v}{\partial r}, \tag{2.12}$$

where η^v is a viscous correction to η and ϕ^v is proportional to μ_l and ϕ_a^v is proportional to μ_a.

The viscous corrections may now be inserted into (2.4). They give rise to uncompensated shear stress proportional to the square of the viscosities which may be removed by new pressure corrections now proportional to the square of viscosities. In this we may generate, successively, irrotational solutions proportional to increasing powers of viscosity.

Though these higher order viscous irrotational contributions vanish rapidly at higher Reynolds numbers, we believe that only the first pressure contribution is of physical significance.

3. Irrotational theory

The governing Navier–Stokes equations and interface conditions for disturbances of the cylinder and gas are made dimensionless with the following scales:

$$[\text{length, velocity, time, pressure}] = \left[2a, U, \frac{2a}{U}, \rho U^2\right]. \tag{3.1}$$

In terms of this normalization, we may define Weber number W, Reynolds number R, density ratio ℓ and viscosity ratio m:

$$W=\frac{\gamma}{\rho 2aU^2},\quad R=\frac{U2a}{\nu},\quad \ell=\frac{\rho_a}{\rho},\quad m=\frac{\mu_a}{\mu}, \tag{3.2}$$

where γ is the surface tension coefficient, $\nu=\mu/\rho$, $\nu_a=\mu_a/\rho_a$ and $m/\ell=\nu_a/\nu$. The azimuthal mode is denoted by n; the $n=0$ mode is axisymmetric and the $n>0$ mode is asymmetric.

This problem for $n=0$ is a combination of capillary instability and Kelvin–Helmholtz instability. When $W=0$ ($\gamma=0$) the instability is generated by the velocity difference. An interesting feature of this instability is that even though the density and viscosity of the gas is much smaller than the liquid, the dynamical effects of the gas cannot be neglected. The relevant physical quantity is the kinematic viscosity $\nu=\mu/\rho$; Funada and Joseph (2001) found that the stability limit for viscous potential flow is nearly independent of the viscosity when $\nu_l>\nu_a$, with a sensible dependence when $\nu_l<\nu_a$, for small viscosities, the opposite of what intuition would suggest. Essentially the same result holds for Kelvin–Helmholtz of liquid jet, studied here. The other limit $W\to\infty$ or $U\to 0$ leads to capillary instability which was studied using viscous potential flow, by Funada and Joseph (2002). Our scaling fails when U tends to zero; in the case the scale velocity is γ/μ, which is the characteristic velocity for capillary collapse and the relevant Reynolds number is $J=\rho\gamma 2a/\mu^2$. The basic flow in dimensionless coordinates is $(\partial\Phi/\partial z,\partial\Phi_a/\partial z)=(1,0)$ in terms of the velocity potential Φ and Φ_a.

3.1. Governing equation

For the liquid cylinder in a disturbed state ($0\leqslant r<1/2+\eta$ and $-\infty<z<\infty$), the velocity potential $\phi\equiv\phi(r,\theta,z,t)$ of an asymmetric disturbance satisfies the Laplace equation:

$$\left(\frac{\partial^2}{\partial r^2}+\frac{1}{r}\frac{\partial}{\partial r}+\frac{1}{r^2}\frac{\partial^2}{\partial\theta^2}+\frac{\partial^2}{\partial z^2}\right)\phi=0 \tag{3.3}$$

and the Bernoulli equation:

$$\frac{\partial\phi}{\partial t}+\frac{\partial\phi}{\partial z}+\frac{1}{2}\left(\frac{\partial\phi}{\partial r}\right)^2+\frac{1}{2}\left(\frac{1}{r}\frac{\partial\phi}{\partial\theta}\right)^2+\frac{1}{2}\left(\frac{\partial\phi}{\partial z}\right)^2+p=f(t), \tag{3.4}$$

where $p\equiv p(r,\theta,z,t)$ is the pressure, and $f(t)$ is an arbitrary function of time t which may be put to zero. For the gas disturbance of infinite extent ($1/2+\eta<r<\infty$ and $-\infty<z<\infty$), the velocity potential $\phi_a\equiv\phi_a(r,\theta,z,t)$ satisfies the equations:

$$\left(\frac{\partial^2}{\partial r^2}+\frac{1}{r}\frac{\partial}{\partial r}+\frac{1}{r^2}\frac{\partial^2}{\partial\theta^2}+\frac{\partial^2}{\partial z^2}\right)\phi_a=0, \tag{3.5}$$

$$\ell\left[\frac{\partial\phi_a}{\partial t}+\frac{1}{2}\left(\frac{\partial\phi_a}{\partial r}\right)^2+\frac{1}{2}\left(\frac{1}{r}\frac{\partial\phi_a}{\partial\phi}\right)^2+\frac{1}{2}\left(\frac{\partial\phi_a}{\partial z}\right)^2\right]+p_a=f_a(t). \tag{3.6}$$

The kinematic condition at the interface $r=1/2+\eta$ is given for each fluid by

$$\frac{\partial\eta}{\partial t}+\frac{\partial\eta}{\partial z}+\frac{1}{(1/2+\eta)^2}\frac{\partial\phi}{\partial\theta}\frac{\partial\eta}{\partial\theta}+\frac{\partial\phi}{\partial z}\frac{\partial\eta}{\partial z}=\frac{\partial\phi}{\partial r},\quad \frac{\partial\eta}{\partial t}+\frac{1}{(1/2+\eta)^2}\frac{\partial\phi_a}{\partial\theta}\frac{\partial\eta}{\partial\theta}+\frac{\partial\phi_a}{\partial z}\frac{\partial\eta}{\partial z}=\frac{\partial\phi_a}{\partial r} \tag{3.7}$$

and the normal stress balance at $r = 1/2 + \eta$ is given by

$$p - p_a - \frac{1}{R}\tau + \frac{m}{R}\tau_a = -W\left[2 - \left[1 + \left(\frac{\partial\eta}{\partial z}\right)^2\right]\left(\frac{1}{1/2+\eta} - \frac{1}{(1/2+\eta)^2}\frac{\partial^2\eta}{\partial\theta^2}\right) + \left[1 + \left(\frac{1}{1/2+\eta}\frac{\partial\eta}{\partial\theta}\right)^2\right]\frac{\partial^2\eta}{\partial z^2} - 2\frac{\partial\eta}{\partial\theta}\left[\frac{1}{(1/2+\eta)^3}\frac{\partial\eta}{\partial\theta} + \frac{1}{(1/2+\eta)^2}\frac{\partial\eta}{\partial z}\frac{\partial^2\eta}{\partial\theta\partial z}\right]\right] \Bigg/ \left[1 + \left(\frac{1}{1/2+\eta}\frac{\partial\eta}{\partial\theta}\right)^2 + \left(\frac{\partial\eta}{\partial z}\right)^2\right]^{3/2}, \tag{3.8}$$

where the pressures at the interface are expressed by (3.4) and (3.6), and τ and τ_a denote the normal viscous stresses acting on the interface:

$$\tau = 2\left[\frac{\partial^2\phi}{\partial r^2} - \frac{1}{1/2+\eta}\frac{\partial\eta}{\partial\theta}\left(\frac{2}{r}\frac{\partial^2\phi}{\partial r\partial\theta} - \frac{2}{r^2}\frac{\partial\phi}{\partial\theta}\right) - \frac{\partial\eta}{\partial z}2\frac{\partial^2\phi}{\partial r\partial z} + \left(\frac{1}{1/2+\eta}\frac{\partial\eta}{\partial\theta}\right)^2\left(\frac{1}{r^2}\frac{\partial^2\phi}{\partial\theta^2} + \frac{1}{r}\frac{\partial\phi}{\partial r}\right) + \frac{1}{1/2+\eta}\frac{\partial\eta}{\partial\theta}\frac{\partial\eta}{\partial z}\frac{2}{r}\frac{\partial^2\phi}{\partial\theta\partial z} + \left(\frac{\partial\eta}{\partial z}\right)^2\frac{\partial^2\phi}{\partial z^2}\right] \times \left[1 + \left(\frac{1}{1/2+\eta}\frac{\partial\eta}{\partial\theta}\right)^2 + \left(\frac{\partial\eta}{\partial z}\right)^2\right]^{-1}, \tag{3.9}$$

$$\tau_a = 2\left[\frac{\partial^2\phi_a}{\partial r^2} - \frac{1}{1/2+\eta}\frac{\partial\eta}{\partial\theta}\left(\frac{2}{r}\frac{\partial^2\phi_a}{\partial r\partial\theta} - \frac{2}{r^2}\frac{\partial\phi_a}{\partial\theta}\right) - \frac{\partial\eta}{\partial z}2\frac{\partial^2\phi_a}{\partial r\partial z} + \left(\frac{1}{1/2+\eta}\frac{\partial\eta}{\partial\theta}\right)^2\left(\frac{1}{r^2}\frac{\partial^2\phi_a}{\partial\theta^2} + \frac{1}{r}\frac{\partial\phi_a}{\partial r}\right) + \frac{1}{1/2+\eta}\frac{\partial\eta}{\partial\theta}\frac{\partial\eta}{\partial z}\frac{2}{r}\frac{\partial^2\phi_a}{\partial\theta\partial z} + \left(\frac{\partial\eta}{\partial z}\right)^2\frac{\partial^2\phi_a}{\partial z^2}\right] \times \left[1 + \left(\frac{1}{1/2+\eta}\frac{\partial\eta}{\partial\theta}\right)^2 + \left(\frac{\partial\eta}{\partial z}\right)^2\right]^{-1}. \tag{3.10}$$

For a case of the interface displacement small compared with the mean radius, (3.7)–(3.10) may be expanded around $r = 1/2$ to give a linear system of boundary conditions for small disturbances. We do not require the continuity of tangential velocity and shear stress. The other conditions are that the liquid velocity is finite at the center $r = 0$, and the gas velocity should vanish as $r \to \infty$.

3.2. Dispersion relation

The potentials ϕ and ϕ_a are determined by the Laplace equation; $\nabla^2\phi = 0$ in $0 \leqslant r < 1/2$ and $\nabla^2\phi_a = 0$ in $1/2 < r$, in terms of cylindrical frame (r, θ, z). The solutions and the surface displacement η are of the form

$$\phi = A_l I_n(kr)E + \text{c.c.}, \quad \phi_a = A_a K_n(kr)E + \text{c.c.}, \quad \eta = AE + \text{c.c.}, \tag{3.11}$$

where A, A_l and A_a are the complex amplitudes, $E \equiv \exp(\mathrm{i}kz + \mathrm{i}n\theta - \mathrm{i}\omega t)$, $\omega \equiv \omega_R + \mathrm{i}\omega_I$ denotes the complex angular frequency, k the real wave number, n is the azimuthal mode and c.c. stands for the complex conjugate of the preceding expression; $I_n(kr)$ and $K_n(kr)$ denote the nth order of

modified Bessel functions of the first and second kind, and the prime denotes the derivative: $I_n'(kr) = \mathrm{d}I_n(kr)/\mathrm{d}(kr)$. Then ϕ gives the finite velocity at $r = 0$ and the velocity $\nabla\phi_a$ vanishes as $r \to \infty$. The solutions satisfy the kinematic conditions at $r = 1/2$

$$\frac{\partial\eta}{\partial t} + \frac{\partial\eta}{\partial z} = \frac{\partial\phi}{\partial r}, \quad \frac{\partial\eta}{\partial t} = \frac{\partial\phi_a}{\partial r}, \tag{3.12}$$

in which (3.11) is substituted to give

$$A_l = \frac{-\mathrm{i}(\omega - k)}{kI_n'(k/2)}A, \quad A_a = \frac{-\mathrm{i}\omega}{kK_n'(k/2)}A. \tag{3.13}$$

To form the normal stress balance we must first solve equation (2.6). We obtain the two pressure corrections

$$-p_l^v = \sum_{j=0}^{\infty} C_j' \mathrm{i}I_n\left(\frac{2\pi}{\lambda}jr\right)\exp\left(\mathrm{i}\frac{2\pi}{\lambda}jz - \mathrm{i}\omega t + \mathrm{i}n\theta\right), \tag{3.14}$$

$$-p_a^v = \sum_{j=0}^{\infty} D_j' \mathrm{i}K_n\left(\frac{2\pi}{\lambda}jr\right)\exp\left(\mathrm{i}\frac{2\pi}{\lambda}jz - \mathrm{i}\omega t + \mathrm{i}n\theta\right), \tag{3.15}$$

where C_j' and D_j' are constants to be determined, j is an integer and λ is the period in the z-direction. Suppose $2\pi j_0/\lambda = k$, $C_{j_0}' = C_k$ and $D_{j0}' = D_k$, then the two pressure corrections can be written as

$$-p_l^v = C_k \mathrm{i}I_n(kr)\exp(\mathrm{i}kz - \mathrm{i}\omega t + \mathrm{i}n\theta) + \sum_{j\neq j_0} C_j' \mathrm{i}I_n\left(\frac{2\pi}{\lambda}jr\right)\exp\left(\mathrm{i}\frac{2\pi}{\lambda}jz - \mathrm{i}\omega t + \mathrm{i}n\theta\right), \tag{3.16}$$

$$-p_a^v = D_k \mathrm{i}K_n(kr)\exp(\mathrm{i}kz - \mathrm{i}\omega t + \mathrm{i}n\theta) + \sum_{j\neq j_0} D_j' \mathrm{i}K_n\left(\frac{2\pi}{\lambda}jr\right)\exp\left(\mathrm{i}\frac{2\pi}{\lambda}jz - \mathrm{i}\omega t + \mathrm{i}n\theta\right), \tag{3.17}$$

With the pressure corrections, the normal stress balance has the following form:

$$p_a^i + p_a^v - p_l^i - p_l^v + \frac{2}{R}\frac{\partial^2\phi}{\partial r^2} - \frac{2m}{R}\frac{\partial^2\phi_a}{\partial r^2} = -W(k^2 + 4n^2 - 4)\eta, \tag{3.18}$$

which gives rise to

$$\begin{aligned}&\ell\mathrm{i}A_a\omega K_n(k/2) - \mathrm{i}A_l(\omega - k)I_n(k/2) - \mathrm{i}D_k K_n(k/2) + \mathrm{i}C_k I_n(k/2) + \frac{2k^2}{R}A_l I_n''(k/2)\\ &\quad + \frac{2mk^2}{R}A_a K_n''(k/2) + \sum_{j\neq j_0}\left[C_j'\mathrm{i}I_n\left(\frac{\pi}{\lambda}j\right) - D_j'\mathrm{i}K_n\left(\frac{\pi}{\lambda}j\right)\right]\exp\left(\mathrm{i}\frac{2\pi}{\lambda}jz - \mathrm{i}\omega t + \mathrm{i}n\theta\right)\\ &\quad = -\frac{\mathrm{i}A_l k}{\omega - k}W(k^2 + 4n^2 - 4)I_n'(k/2).\end{aligned} \tag{3.19}$$

By orthogonality of the Fourier series, we obtain

$$\begin{aligned}&\ell A_a\omega K_n(k/2) - A_l(\omega - k)I_n(k/2) - D_k K_n(k/2) + C_k I_n(k/2)\\ &\quad - \mathrm{i}\frac{2k^2}{R}A_l I_n''(k/2) - \mathrm{i}\frac{2mk^2}{R}A_a K_n''(k/2) = -\frac{A_l k}{\omega - k}W(k^2 + 4n^2 - 4)I_n'(k/2)\end{aligned} \tag{3.20}$$

and

$$C'_j I_n\left(\frac{\pi}{\lambda}j\right) - D'_j K_n\left(\frac{\pi}{\lambda}j\right) = 0 \quad \text{when } j \neq j_0. \tag{3.21}$$

Eq. (3.20) replaces the normal stress balance and can be solved for the growth rate ω. However, the undetermined part $C_k I_n(k/2) - D_k K_n(k/2)$ has to be computed from (2.5) before we can solve (3.20). Substitution of (3.16), (3.17) and (3.21) into the left hand side of (2.5) gives rise to

$$\begin{aligned}\int_\Omega \bar{u}_n(-p_l^v + p_a^v)\,\mathrm{d}\Omega &= \int_o^{2\pi} \frac{1}{2}\mathrm{d}\theta \int_z^{z+\lambda} \bar{u}_n(-p_l^v + p_a^v)\,\mathrm{d}z \\ &= \pi\lambda[\bar{A}_l C_k I_n(k/2) I'_n(k/2) - \bar{A}_a D_k K_n(k/2) K'_n(k/2)]\,\mathrm{i}kE\bar{E},\end{aligned} \tag{3.22}$$

where $\bar{u}_n$ is the conjugate of u_n. The right hand side of (2.5) can be evaluated

$$\int_\Omega [(\overline{\boldsymbol{u}_l \cdot \boldsymbol{t}})\tau_l^s - (\overline{\boldsymbol{u}_a \cdot t})\tau_a^s]\,\mathrm{d}\Omega = \pi\lambda\left[\frac{2}{R}\bar{A}_l A_l I_n(k/2) I'_n(k/2) - \frac{2m}{R}\bar{A}_a A_a K_n(k/2) K'_n(k/2)\right] k^3 E\bar{E}. \tag{3.23}$$

Combining (3.22) and (3.23), we obtain

$$\begin{aligned}&\bar{A}_l C_k \mathrm{i} I_n(k/2) I'_n(k/2) - \bar{A}_a D_k K_n(k/2) K'_n(k/2) \\ &\quad = \frac{2}{R}\bar{A}_l A_l k^2 I_n(k/2) I'_n(k/2) - \frac{2m}{R}\bar{A}_a A_a k^2 K_n(k/2) K'_n(k/2).\end{aligned} \tag{3.24}$$

Substitution of (3.13) into (3.24) leads to

$$C_k = -\frac{2\mathrm{i}}{R}k^2 A_l, \quad D_k = -\frac{2\mathrm{i}m}{R}k^2 A_a. \tag{3.25}$$

Inserting (3.13) and (3.24) into (3.20), we obtain the dispersion relation

$$(\omega - k)^2 \alpha_{\ell n} + \ell\omega^2 \alpha_{an} + \mathrm{i}\frac{2k^2}{R}(\omega - k)(\beta_{\ell n} + \alpha_{\ell n}) + \mathrm{i}\frac{2mk^2}{R}\omega(\beta_{an} + \alpha_{an}) - W(k^2 + 4n^2 - 4)k = 0, \tag{3.26}$$

where $\alpha_{\ell n}$, α_{an}, $\beta_{\ell n}$ and β_{an} are defined as

$$\alpha_{\ell n} = \frac{I_n(k/2)}{I'_n(k/2)}, \quad \alpha_{an} = -\frac{K_n(k/2)}{K'_n k/2}, \quad \beta_{\ell n} = \frac{I''_n(k/2)}{I'_n(k/2)}, \quad \beta_{an} = -\frac{K''_n(k/2)}{K'_n(k/2)}. \tag{3.27}$$

4. Dissipation calculation for capillary and KH instability

The dissipation method is a way to include viscous effects into solutions assuming potential flows. Joseph and Wang (2004) showed that VCVPF and dissipation method give the same results in a few problems involving free surfaces, such as the drag force on a spherical or oblate ellipsoidal gas bubble, and the decay rate of free gravity waves on water. Wang et al. (2005b) showed that the dissipation calculation gives the same growth rates as VCVPF for capillary instability

involving a gas and a viscous fluid. Here we extend the dissipation calculation to capillary instability of two viscous fluids.

The sum of the mechanical energy equations of the interior and exterior fluids can be written as

$$\int_{V_a} \frac{\ell}{2}\frac{\partial}{\partial t}|\boldsymbol{u}_a|^2\,\mathrm{d}V + \int_{V_l}\frac{1}{2}\left(\frac{\partial}{\partial t}+\frac{\partial}{\partial z}\right)|\boldsymbol{u}_l|^2\,\mathrm{d}V$$
$$= \int_\Omega [u_n(-p_l+\tau_l^n+p_a-\tau_a^n)+\boldsymbol{u}_l\cdot\boldsymbol{t}\tau_l^s-\boldsymbol{u}_a\cdot\boldsymbol{t}\tau_a^s+\boldsymbol{u}_l\cdot\boldsymbol{b}\tau_l^b-\boldsymbol{u}_a\cdot\boldsymbol{b}\tau_a^b]\,\mathrm{d}\Omega$$
$$-\int_{V_a}\frac{2m}{R}\mathbf{D}_a:\mathbf{D}_a\,\mathrm{d}V-\int_{V_i}\frac{2}{R}\mathbf{D}_l:\mathbf{D}_l\,\mathrm{d}V. \tag{4.1}$$

We assume that the normal stress balance

$$p_a-\tau_a^n-p_l+\tau_l^n = W\left(\frac{\partial^2\eta}{\partial z^2}+4\frac{\partial^2\eta}{\partial\theta^2}+4\eta\right) \tag{4.2}$$

and the continuity of the tangential velocity and stress

$$\tau_a^s=\tau_l^s=\tau^s,\quad \boldsymbol{u}_a\cdot\boldsymbol{t}=\boldsymbol{u}_l\cdot\boldsymbol{t}=u_s,\quad \tau_a^b=\tau_l^b=\tau^b,\quad \text{and}\quad \boldsymbol{u}_a\cdot\boldsymbol{b}=\boldsymbol{u}_\ell\cdot\boldsymbol{b}=u_b, \tag{4.3}$$

are all satisfied at the interface. At the same time, the flow in the bulk of the fluids are approximated by potential flow, for which the following identity can be easily proved

$$\int_V 2\mathbf{D}:\mathbf{D}\,\mathrm{d}V=\int_\Omega \boldsymbol{n}\cdot 2\mathbf{D}\cdot\boldsymbol{u}\,\mathrm{d}\Omega, \tag{4.4}$$

where Ω is the surface of V and $\boldsymbol{n}$ is the unit normal pointing outward. Inserting (4.2)–(4.4) into (4.1), we obtain

$$\int_{V_a}\frac{\ell}{2}\frac{\partial}{\partial t}|\boldsymbol{u}_a|^2\,\mathrm{d}V=\int_{V_l}\frac{1}{2}\left(\frac{\partial}{\partial t}+\frac{\partial}{\partial z}\right)|\boldsymbol{u}_l|^2\,\mathrm{d}V$$
$$=\int_\Omega u_n W\left(\frac{\partial^2\eta}{\partial z^2}+4\frac{\partial^2\eta}{\partial\theta^2}+4\eta\right)\mathrm{d}\Omega$$
$$+\frac{m}{R}\int_\Omega n_1\cdot 2D_a\cdot\boldsymbol{u}_a\mathrm{d}\Omega-\frac{1}{R}\int_\Omega \boldsymbol{n}_1\cdot 2\mathbf{D}_l\cdot\boldsymbol{u}_l\,\mathrm{d}\Omega. \tag{4.5}$$

The integrals in (4.5) are evaluated

$$\int_{V_l}\frac{1}{2}\left(\frac{\partial}{\partial t}+\frac{\partial}{\partial z}\right)|\boldsymbol{u}_l|^2\,\mathrm{d}V=\int_0^{2\pi}\mathrm{d}\theta\int_z^{z+\lambda}\int_0^{\frac{1}{2}}\frac{1}{2}\left(\frac{\partial}{\partial t}+\frac{\partial}{\partial z}\right)|\boldsymbol{u}_l|^2 r\,\mathrm{d}r\,\mathrm{d}z$$
$$=\frac{1}{2}|A_1|^2\pi\lambda k I_n(k/2)I_n'(k/2)(\sigma+\bar\sigma)\exp(\sigma+\bar\sigma)t, \tag{4.6}$$

$$\int_{V_a}\frac{\ell}{2}\frac{\partial}{\partial t}|\boldsymbol{u}_a|^2\,\mathrm{d}V=\int_0^{2\pi}\mathrm{d}\theta\int_z^{z+\lambda}\int_{\frac{1}{2}}^{\infty}\frac{\ell}{2}\frac{\partial}{\partial t}|\boldsymbol{u}_a|^2 r\,\mathrm{d}r\,\mathrm{d}z$$
$$=\frac{1}{2}\ell|B_1|^2\pi\lambda k K_n(k/2)K_n'(k/2)(\sigma+\bar\sigma)\exp(\sigma+\bar\sigma)t, \tag{4.7}$$

$$\int_\Omega W\left(\frac{\partial^2\eta}{\partial z^2}+4\frac{\partial^2\eta}{\partial\theta^2}+4\eta\right)u_l\,\mathrm{d}\Omega=|A_1|^2\pi\lambda W\frac{k^2}{\sigma}I_n'^2(k/2)(4-4n^2-k^2)\exp(\sigma+\bar\sigma)t, \tag{4.8}$$

$$\frac{1}{R}\int_\Omega \boldsymbol{n}_1\cdot 2\mathbf{D}_l\cdot\boldsymbol{u}_l\,\mathrm{d}\Omega=\frac{2}{R}|A_1|^2\pi\lambda k^3 I_n'(k/2)\left[2I_n(k/2)-\frac{I_n'(k/2)}{k/2}\right]\exp(\sigma+\bar\sigma)t, \tag{4.9}$$

$$\frac{m}{R}\int_\Omega \boldsymbol{n}_1\cdot 2\mathbf{D}_a\cdot\boldsymbol{u}_a\,\mathrm{d}\Omega=\frac{2m}{R}|A_1|^2\pi\lambda k^3 K_n'(k/2)\left[2K_n(k/2)+\frac{K_n'(k/2)}{k/2}\right]\exp(\sigma+\bar\sigma)t. \tag{4.10}$$

Inserting (4.6)–(4.10) into (4.5), we obtain

$$(\alpha_{\ell n}+\ell\alpha_{an})\frac{\sigma+\bar\sigma}{2}+\frac{2k^2}{R}[(\beta_{\ell n}+\alpha_{\ell n})+m(\beta_{an}+\alpha_{an})]=W\left(4-4n^2-k^2\right)\frac{k}{\sigma}, \tag{4.11}$$

where $\alpha_{\ell n}$, α_{an}, $\beta_{\ell n}$ and β_{an} are defined in (3.27). If we assume that σ is real, (4.11) is the same as the dispersion relation (3.26) from the VCVPF solution. In the range $0<k\leqslant 1/R=2$ when $W^{-1}=0$, σ is real and our assumption is satisfied. Therefore, the growth rate computed by the dissipation calculation is the same as that computed by the VCVPF.

5. Small and large wave number defined by the asymptotic expansion of Bessel functions

We first note that the Bessel functions in our dispersion equation (3.26) appear only in the ratios $\alpha_{\ell n}$, α_{an}, $\beta_{\ell n}$, β_{an} which are functions of k and n as shown in (3.27). In small k expansion, the leading terms for these expressions are

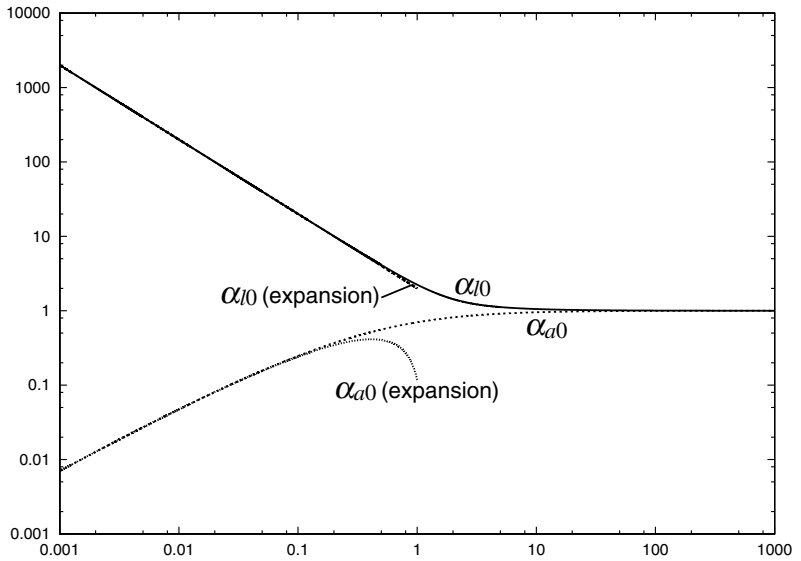

Fig. 1. $\alpha_{\ell 0}$, its small k expansion, α_{a0} and its small k expansion versus k. The small k expansions approximate well $\alpha_{\ell 0}$ and α_{a0} in $0<k<2$. Such expansion holds for $\alpha_{\ell 1}$, α_{a1}, $\beta_{\ell n}$ and β_{an} with $n=0$, 1. For large k ($k>10$), we can find that $\alpha_{\ell n}$, α_{an}, $\beta_{\ell n}$, $\beta_{an}=1$ for any n.

$$\alpha_{\ell 0} = -\frac{I_0(x)}{I_0'(x)} = \frac{2}{x} + \mathrm{O}(x), \quad \alpha_{\ell 1} = \frac{I_1(x)}{I_1'(x)} = x + \mathrm{O}(x^3), \tag{5.1}$$

$$\alpha_{a0} = -\frac{K_0(x)}{K_0'(x)} = (-\gamma + \log(2) - \log(x))x + \mathrm{O}(x^3), \quad \alpha_{a1} = -\frac{K_1(x)}{K_1'(x)} = x + \mathrm{O}(x^3), \tag{5.2}$$

$$\beta_{a0} = -\frac{I_0''(x)}{I_0'(x)} = \frac{1}{x} + \mathrm{O}(x), \quad \beta_{\ell 1} = \frac{I_1''(x)}{I_0'(x)} = \frac{3x}{4} + \mathrm{O}(x^3), \tag{5.3}$$

$$\beta_{a0} = -\frac{K_0''(x)}{K_0'(x)} = \frac{1}{x} + \mathrm{O}(x), \quad \beta_{a1} = -\frac{K_1''(x)}{K_1'(x)} = \frac{2}{x} + \mathrm{O}(x), \tag{5.4}$$

where $\gamma = 0.577216$ is Euler's constant and $x = k/2$. This small k expansions give good representations of the ratios when $k < 2$ (see Fig. 1). The graphs of these Bessel function ratios lead to one when k is large independent of n and are very nearly one for $k > 2$.

6. Properties of the dispersion relation

For brevity we denote as

$$B_{\ell n} = \beta_{\ell n} + \alpha_{\ell n}, \quad B_{an} = \beta_{an} + \beta_{an}, \tag{6.1}$$

which reminds us of VPF when $B_{\ell n} = \beta_{\ell n}$ and $B_{an} = \beta_{an}$. The dispersion relation is then expressed in the quadratic equation in $\omega = \omega_R + \mathrm{i}\omega_I$

$$D(k,\omega) = c_2\omega^2 + 2c_1\omega + c_0 = 0 \ \rightarrow \ (c_2\omega + c_1)^2 = c_1^2 - c_2c_0, \tag{6.2}$$

where

$$c_2 = \alpha_{\ell n} + \ell\alpha_{an}, \tag{6.3}$$

$$c_1 = -k\alpha_{\ell n} + \mathrm{i}\frac{k^2}{R}(B_{\ell n} + mB_{an}) = C_{1R} + \mathrm{i}c_{1I}, \tag{6.4}$$

$$c_0 = k^2\alpha_{\ell n} - \mathrm{i}\frac{2k^3}{R}B_{\ell n} - W(k^2 + 4n^2 - 4)k = c_{0R} + \mathrm{i}c_{0I}. \tag{6.5}$$

Putting as

$$c_2\omega + c_1 = c_2(\omega_R + \mathrm{i}\omega_I) + c_{1R} + \mathrm{i}c_{1I} = X + \mathrm{i}Y, \tag{6.6}$$

we have

$$\begin{aligned}(X + \mathrm{i}Y)^2 &= X^2 - Y^2 + 2\mathrm{i}XY = (C_{1R} + \mathrm{i}c_{1I})^2 - c_2(c_{0R} + \mathrm{i}c_{0I}) \\ &= c_{1R}^2 - c_{1I}^2 - c_2c_{0R} + \mathrm{i}(2c_{1R}c_{1I} - c_2c_{0I}),\end{aligned}$$

then

$$X^2 - Y^2 = c_{1R}^2 - c_{1I}^2 - c_2c_{0R}, \quad 2XY = 2c_{1R}c_{1I} - c_2c_{0I}. \tag{6.7}$$

Thus the equation for $X = c_2\omega_R + c_{1R}$ is given by the quadratic in X^2

$$X_2 - \frac{(c_{1R}c_{1I} - c_2c_{0I}/2)^2}{X^2} = c_{1R}^2 - c_{1I}^2 - c_2c_{0R} \tag{6.8}$$

and the equation for $Y = c_2\omega_I + c_{1I}$ is given by the quadratic in Y^2

$$\frac{(c_{1R}c_{1I} - c_2c_{0I}/2)^2}{Y^2} - Y^2 = c_{1R}^2 - c_{1I}^2 - c_2c_{0R}. \tag{6.9}$$

6.1. Cut-off wave number $k = k_c$

All waves with $k > k_c$ are damped. Moreover k_c is independent of R; it depends on W^{-1}, ℓ and m. $k = k_c$ is a root of $\omega_I = 0$ for which $Y = c_{1I}$, we have

$$\frac{(c_{1R}c_{1I} - c_2c_{0I}/2)^2}{c_{1I}^2} - C_{1I}^2 = c_{1R}^2 - c_{1I}^2 - c_2c_{0R} \;\rightarrow\; -c_{1R}c_{1I}c_{0I} + \frac{1}{4}c_2c_0^2 + c_{1I}^2c_{0R} = 0, \tag{6.10}$$

which is then arranged as

$$\frac{k^6}{R^2}\left\{\left[\ell\alpha_{an}(\beta_{\ell n} + \alpha_{\ell n})^2 + m^2\alpha_{\ell n}(\beta_{an} + \alpha_{an})^2\right] - [(\beta_{\ell n} + \alpha_{\ell n}) + m(\beta_{an} + \alpha_{an})]^2 \frac{W}{k}(k^2 + 4n^2 - 4)\right\} = 0, \tag{6.11}$$

thus we have the equation to the cut-off wave number $k = k_c$ for VCVPF

$$W^{-1} = \frac{[(\beta_{\ell n} + \alpha_{\ell n}) + m(\beta_{an} + \alpha_{an})]^2}{\ell\alpha_{an}(\beta_{\ell n} + \alpha_{\ell n})^2 + m^2\alpha_{\ell n}(\beta_{an} + \beta_{an})^2}\frac{1}{k}(k^2 + 4n^2 - 4) \tag{6.12}$$

and for VPF

$$W^{-1} = \frac{(\beta_{\ell n} + m\beta_{an})^2}{\ell\alpha_{an}\beta_{\ell n}^2 + m^2\alpha_{\ell n}\beta_{an}^2 k}\frac{1}{k}(k^2 + 4n^2 - 4). \tag{6.13}$$

In $0 < k < k_c$ instability may arise, for which the maximum growth rate ω_{Im} can be defined by $\omega_{Im} \stackrel{\text{def}}{=} \text{Max}(\omega_I(k))$ with the associated wave number k_m. We are $k_m < 2$ for which the small k expansions are uniformly valid. Since $k_m < k_c$, the validity can be expected when k_c is not too much larger than 2. Eqs. (6.12) and (6.13) show that k_c is not much larger than 2 when $W^{-1} < 10{,}000$ and $k_c \approx 2$ or $k_c < 2$ when $W^{-1} < 1000$ (see Fig. 2).

For $k > 10$ for which $\alpha_{\ell n}$, α_{an}, $\beta_{\ell n}$, $\beta_{an} = 1$, we have the following asymptotic relation of W^{-1} and k_c for both VPF and VCVPF:

$$W^{-1} = \frac{(1+m)^2}{\ell + m^2}\frac{1}{k}(k^2 + 4n^2 - 4) \approx \frac{(1+m)^2}{\ell + m^2}k \;\rightarrow\; W^{-1} = \frac{(1+m)^2}{\ell + m^2}k_c. \tag{6.14}$$

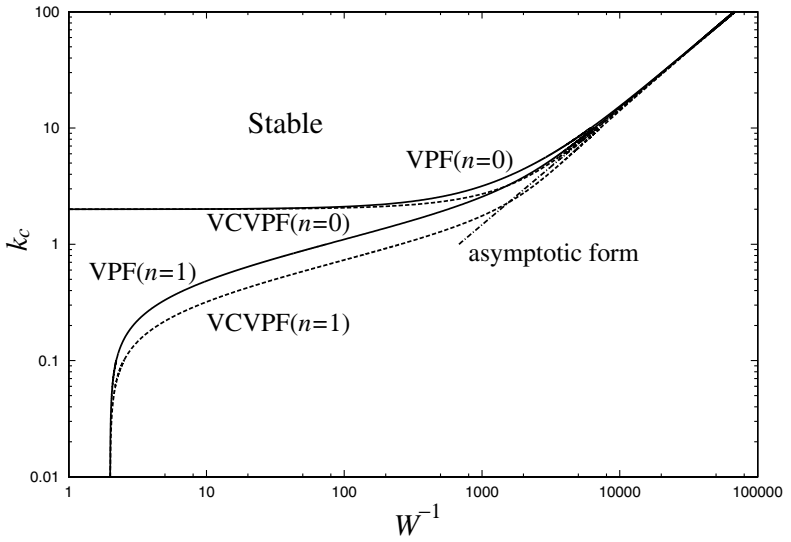

Fig. 2. Cut-off wave number $k = k_c$ versus W^{-1} for water–air with $\ell = 0.0012$ and $m = 0.018$; VPF (solid line) and VCVPF (dotted line). The left top region denotes "stable." In the axisymmetric case of $n = 0$, the disturbance in $k < k_c = 2$ is always unstable due to the capillary instability. The first asymmetric disturbance ($n = 1$) is stable when $W^{-1} < W_{c1}^{-1} = 2$ in both VPF and VCVPF, where $W_{c1} = 1/2$ is the critical Weber number below which the disturbances grow in time. Away from the curves the right hand side denotes "unstable region." The asymptotic form (6.14) is also shown, which is irrespective of n for $k > 10$.

6.2. Large k expansion of the dispersion relation

The term $c_1^2 - c_2 c_0$ in (6.2) is arranged as

$$c_1^2 - c_2 c_0 = -\ell k^2 \alpha_{\ell n}\alpha_{an} - \frac{k^4}{R^2}(B_{\ell n} + mB_{an})^2 + \frac{\mathrm{i}2k^3}{R}(\ell\alpha_{an}B_{\ell n} - m\alpha_{\ell n}B_{an}) + (\alpha_{\ell n} + \ell\alpha_{an})W(k^2 + 4n^2 - 4)k, \tag{6.15}$$

which is real in a special case that $(\ell\alpha_{an}B_{\ell n} - m\alpha_{\ell n}B_{an}) = 0$.

When $k > 10$, KH instability dominates and Eq. (6.1) shows that

$$\begin{aligned} &B_{\ell n} = B_{an} = 1 \quad \text{for VPF},\\ &B_{\ell m} = B_{am} = 1 \quad \text{for VCVPF}. \end{aligned} \tag{6.16}$$

Eq. (6.16) shows that the dispersion relation for VPF at a Reynolds number R is the same as for VCVPF at a Reynolds number $2R$. The solution $X + \mathrm{i}\,Y$ in (6.6)–(6.9) is

$$X = c_2\omega_R + c_{1R} = \pm\Re\left\{\sqrt{c_1^2 - c_2 c_0}\right\}, \quad Y = c_2\omega_I + c_{1I} = \pm\Im\left\{\sqrt{c_1^2 - c_2 c_0}\right\}. \tag{6.17}$$

When $\ell = m$ in (6.17) and the discriminant is not negative, ω_I and ω_R can be expressed as

$$\omega_I + \frac{k_2}{R} = \pm\sqrt{\frac{\ell k^2}{(1+\ell)^2} + \frac{k^4}{R^2} - W\frac{(k^2+4n^2-4)k}{(1+\ell)}}, \quad \omega_R = \frac{k}{1+\ell} \quad \text{for VPF}, \tag{6.18}$$

$$\omega_I + \frac{2k^2}{R} = \pm\sqrt{\frac{\ell k^2}{(1+\ell)^2} + \frac{4k^4}{R^2} - W\frac{(k^2+4n^2-4)k}{(1+\ell)}}, \quad \omega_R = \frac{k}{1+\ell} \quad \text{for VCVPF}. \tag{6.19}$$

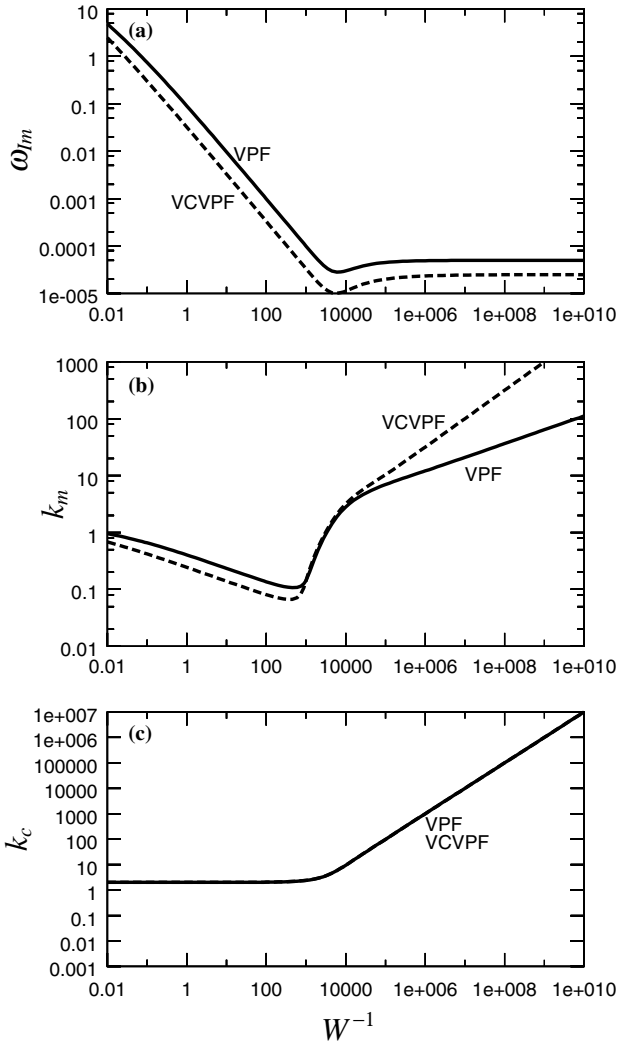

Fig. 3. ω_{Im}, k_m and k_c versus W^{-1} for the axisymmetric disturbances ($n = 0$), $R = 0.1$, $\ell = m = 10^{-3}$; VPF (solid line), VCVPF (dotted line). Capillary instability dominates in $W^{-1} < 10^4$ and $k < 2$, while KH instability in $W^{-1} > 10^4$ and $k > 10$. The large k expansion may be applied well when $k_m > 10$ and $k_c > 10$; the KH instability may give rise to small size drops.

If there holds an extremum condition that $\partial\omega_i/\partial k = 0$, (6.19) for VCVPF gives

$$\frac{4k}{R}\left(\omega_I + \frac{2k^2}{R}\right) = \frac{2\ell k}{(1+\ell)^2} + \frac{16k^3}{R^2} - W\frac{(3k^2 4n^2 - 4)}{(1+\ell)}, \tag{6.20}$$

which together with (6.19) leads to the maximum growth rate $\omega_I(k_m)$ at $k = k_m$. Fig. 3 shows for the axisymmetric disturbances ($n = 0$) that the capillary instability occurs in $0 < W^1 < 10^4$, while the KH instability in $W^1 > 10^4$ where k_m increases with W^{-1}.

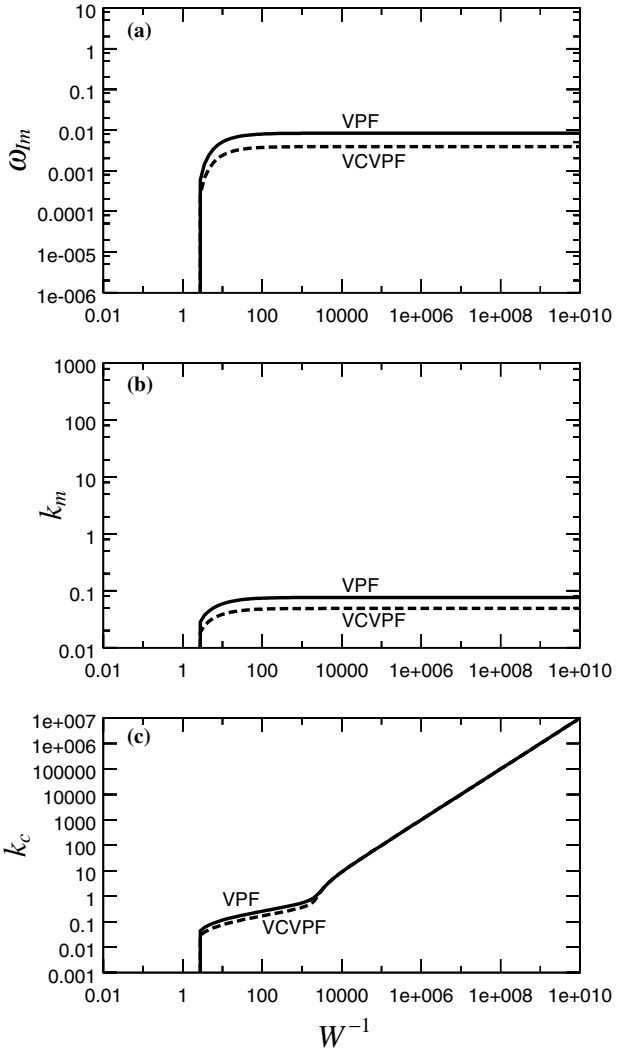

Fig. 4. ω_{Im}, k_m and k_c versus W^{-1} for $n = 1$, $R = 0.1$, $\ell = m = 10^{-3}$; VPF (solid line), VCVPF (dotted line). KH instability occurs in $W^{-1} > W_{c1}^{-1}$ where $W_{c1}^{-1} = 2$ is the critical Weber number. This ω_{Im} is 100 times larger than that in Fig. 3 for $n = 0$, at k_m 100 times smaller than k_m for $n = 0$. The asymmetric disturbance plays a significant role at such small R.

6.3. Small k expansion of the dispersion relation

Using (5.1)–(5.4), the dispersion relation is given in small k; for VPF

$$D(k,\omega;n=0) = (\omega-k)^2\frac{4}{k} + \ell\omega^2\left(-\gamma+\log(2)-\log\left(\frac{k}{2}\right)\right)\frac{k}{2} + \mathrm{i}\frac{2k^2}{R}(\omega-k)\frac{2}{k} + \mathrm{i}\frac{2mk^2}{R}\omega\frac{2}{k} - W(k^2-4)k = 0, \tag{6.21}$$

$$D(k,\omega;n=1) = (\omega-k)^2\frac{k}{2} + \ell\omega^2\frac{k}{2} + \mathrm{i}\frac{2k^2}{R}(\omega-k)\frac{3}{8}k + \mathrm{i}\frac{2mk^2}{R}\omega\frac{4}{k} - Wk^3 = 0 \tag{6.22}$$

and for VCVPF

$$D(k,\omega;n=0) = (\omega-k)^2\frac{4}{k} + \ell\omega^2\left(-\gamma+\log(2)-\log\left(\frac{k}{2}\right)\right)\frac{k}{2} + \mathrm{i}\frac{2k^2}{R}(\omega-k)\frac{6}{k} + \mathrm{i}\frac{2mk^2}{R}\omega\left[\frac{2}{k} + \left(-\gamma+\log(2)-\log\left(\frac{k}{2}\right)\frac{k}{2}\right)\right] - W(k^2-4)k = 0, \tag{6.23}$$

$$D(k,\omega;n=1) = (\omega-k)^2\frac{k}{2} + \ell\omega^2\frac{k}{2} + \mathrm{i}\frac{2k^2}{R}(\omega-k)\frac{7k}{8} + \mathrm{i}\frac{2mk^2}{R}\omega\left(\frac{4}{k}+\frac{k}{2}\right) - Wk^3 = 0. \tag{6.24}$$

Fig. 4 shows for the asymmetric disturbances ($n=1$) that the KH instability occurs in $W^{-1}>2$ where k_m stays less than unity. This k_m about 100 times smaller than k_m for $n=0$ in Fig. 3, makes ω_{Im} 100 times larger than that for $n=0$; long drops may arise due to this KH instability. The small k_m and ω_{Im} for the asymmetric disturbances ($n=1$) can be evaluated well using the small k expansion of the dispersion relation shown above.

7. Large Reynolds number $R > 100$

We get inviscid flow, $n=0$ is the only unstable mode, ω_I depends on W^{-1} and l. There is a critical value $W_c^{-1}(l)$ given by (7.6) at the cut-off wave number $k_c=2$, which gives a border between capillary instability and KH instability (see Fig. 5). When $k<2$, we have $W^{-1}(\ell)$ such that

$$W^{-1}(\ell) < \tilde{W}_c^{-1}(\ell); \tag{7.1}$$

the flow is dominated by capillary instability. When $k>2$, $W^{-1}(\ell)$ is

$$W^{-\ell}(\ell) > \tilde{W}_c^{-1}(\ell); \tag{7.2}$$

the flow is dominated by KH instability.

7.1. Inviscid case

The dispersion relation for $k>10$ and any n ($n=0$, 1) is approximated as

$$(1+\ell)\omega^2 - 2k\omega + k^2 - Wk^3 = 0, \tag{7.3}$$

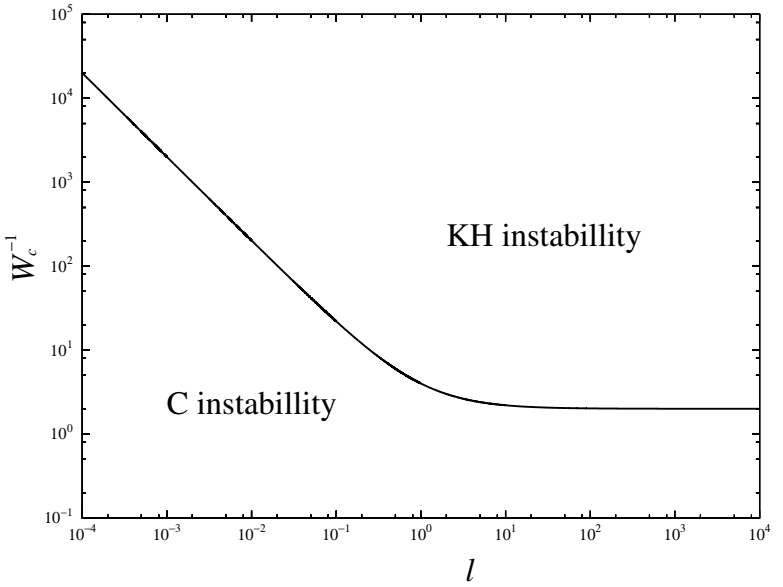

Fig. 5. W_c^{-1} versus ℓ for IPF, which is given by (7.6) with $k_c = 2$. Capillary instability dominates when W^{-1} is small and KH instability dominates when W^{-1} is large. Roughly speaking, small is $W^{-1} < 12{,}000$, large is $W^{-1} > 12{,}000$.

for which the solution is given by

$$\omega = \omega_R + \imath\omega_I = \frac{k}{1+\ell} \pm \imath\sqrt{\frac{\ell k^2}{(1+\ell)^2} - \frac{Wk^3}{1+\ell}}, \tag{7.4}$$

thus

$$\omega_R = \frac{k}{1+\ell}, \quad \omega_I = \pm\sqrt{\frac{\ell k^2}{1+\ell^2} - \frac{Wk^3}{1+\ell}}. \tag{7.5}$$

The growth rate ω_I is put to zero to give the cut-off wave number k_c

$$\omega_I = \pm\sqrt{\frac{\ell k^2}{(1+\ell)^2} - \frac{Wk^3}{1+\ell}} = 0 \ \rightarrow \ k_c = \frac{\ell}{1+\ell} W^{-1}. \tag{7.6}$$

The external value of growth rate should satisfy

$$\frac{\partial \omega_I^2}{\partial k} = \frac{\ell 2k}{(1+\ell)^2} - \frac{Wk^3}{1+\ell} = 0 \ \rightarrow \ k = 0, \quad k = \frac{2}{3}\frac{\ell}{1+\ell} W^{-1} = k_m, \tag{7.7}$$

hence the external value ω_{Im} is given by

$$\omega_{Im} = \omega_I(k_m) = \sqrt{\frac{\ell k_m^2}{(1+\ell)^2} - \frac{Wk^3}{1+\ell}} = \frac{2}{3\sqrt{3}}\frac{\ell\sqrt{\ell}}{(1+\ell)^2} W^{-1}. \tag{7.8}$$

For the large k expansion ($k > 10$), ω_{Im} is given by (7.8), k_m is given by (7.7) and k_c is given by (7.6).

7.2. k_c in inviscid case

In Fig. 6, we have plotted k_c versus W^{-1} for IPF and identified a unique point of intersection $W_*^{-1}(l)$ of the instability modes for $n = 0$ and $n = 1$. The KH instability dominates when W^{-1} is

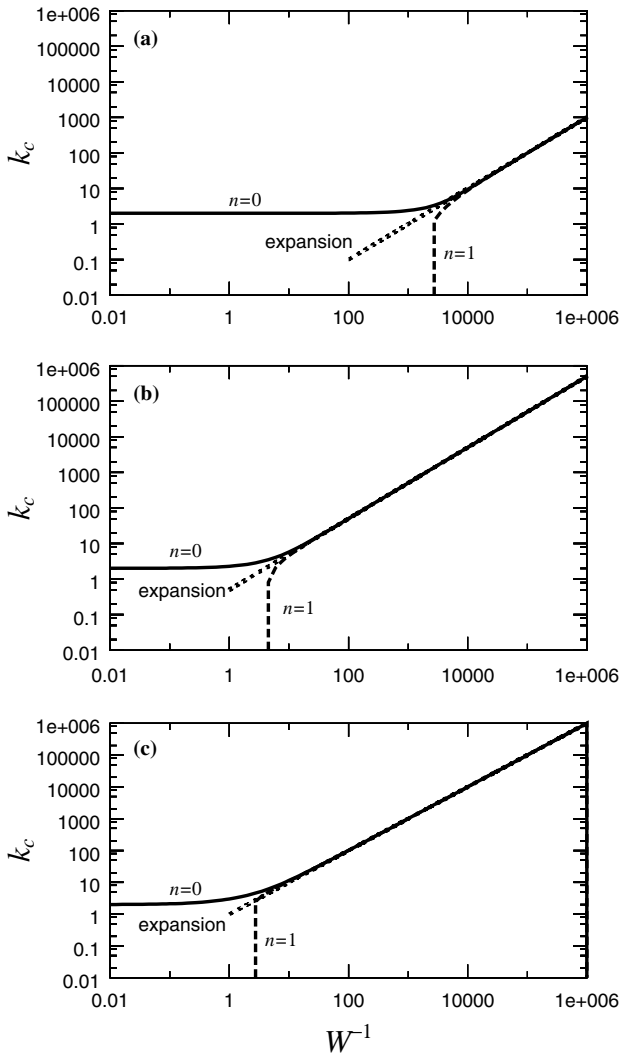

Fig. 6. k_c versus W^{-1} for IPF; $n = 0$ (solid line), $n = 1$ (dashed line), the large k expansion (7.6) (dotted line); $W_*^{-1}(l)$ is given by $W^{-1} = \frac{l+1}{l} k_c$ at $k_c = 10$. (a) $\ell = 10^{-3}$ for which $W_*^{-1} = 10010$, (b) $\ell = 1$ for which $W_*^{-1} = 20$, (c) $\ell = 10^3$ for which $W_*^{-1} = 10.01$.

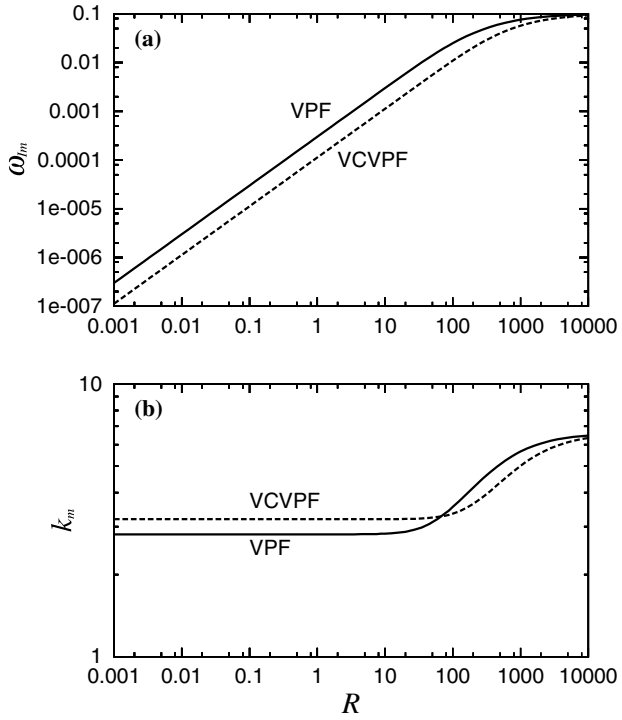

Fig. 7. ω_{Im}, k_m versus R for the axisymmetric disturbances ($n = 0$), $W^{-1} = 10^4$ and $\ell = m = 10^{-3}$. VCVPF and VPF show that the viscous effects arise remarkably at small R and disappear as R becomes large.

greater than the intercept point $W_*^{-1}(l)$ and KH instability dominates when W^{-1} is below this point. W_*^{-1} (l) decreases as l increases.

7.3. KH instability for large R

Setting as $W^{-1} = 10^4$ where KH instability dominates, ω_{Im} and k_m change with increasing R, as in Figs. 7 and 8. VCVPF and VPF show that the viscous effects arise remarkably at small R and disappear as R becomes large. It is noted that the $n = 1$ mode dominates in $R < 100$.

8. Comparison of VPF and VCVPF

The analysis of stability of a liquid jet given by Funada et al. (2004) was based on viscous potential flow (VPF) without an additional viscous pressure correction (VCVPF). Previous studies on related problems have shown that VCVPF is in excellent agreement with exact solutions. We recommend VCVPF for stability analysis in the problem studied here.

We have already shown that the difference between VPF and VCVPF vanishes in the inviscid limit (practically for $R > 100$). The difference between the two theories also vanishes when KH instability is very dominant (large value of W^{-1}) and are sensible when capillary instability

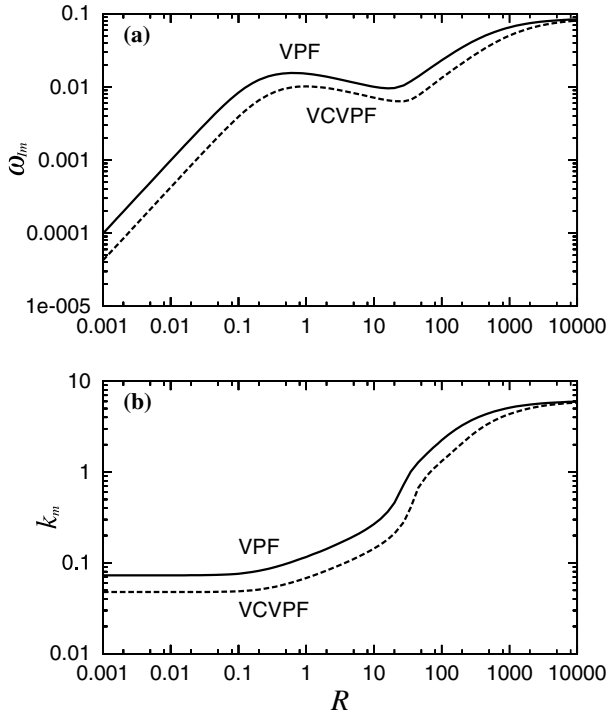

Fig. 8. ω_{Im}, k_m versus R for the asymmetric disturbances ($n = 1$), $W^{-1} = 10^4$ and $\ell = m = 10^{-3}$. The $n = 1$ mode dominates in $R < 100$.

dominants (W^{-1} is small). When capillary instability dominates ($W^{-1} < 1000$) the normalized growth discrepancy

$$\frac{\omega_I^1(k_m^1, \mathrm{VPF}) - \omega_I^2(k_m^2, \mathrm{VCVPF})}{\omega_I^1(k_m^1, \mathrm{VPF})} \approx \mathrm{O}(1/2). \tag{8.1}$$

9. Conclusions

The stability of a liquid jet into viscous incompressible gases and liquids is studied. The analysis assumes that the motion of the fluids is irrotational. In our previous theory (VPF) the viscous component of the normal stress is evaluated on the potential flows (Funada et al. (2004)). Here we construct a new irrotational theory in which the discontinuities of the irrotational tangential velocity and shear stress in the power of traction integrals in the evolution of energy equations is eliminated by the selection of two viscous contributions to the pressure. VCVPF is VPF with pressure corrections. The main results are as follows:

(1) The dispersion relation for VCVPF is the same as the one that arises from the dissipation method.

(2) The variation of the growth rate curves with the Weber and Reynolds number and the density and viscosity ratio are similar for VPF and VCVPF but the values can be different.
(3) The dispersion relations differ from those which arise in the study of capillary instability in terms involving the uniform base flow velocity difference $U = U_i - U_a$.
(4) The problem here must be treated as a two fluid problem even when one fluid is gas, because Kelvin–Helmholtz instability cannot occur in a vacuum.
(5) In both theories the problem is dominated by the Kelvin–Helmholtz instability when the Weber number is small and by capillary instability when it is large.
(6) The flow is always unstable to wave numbers smaller than a cut-off wave number which increases from a small value for Capillary instability to much larger values for Kelvin–Helmholtz instability. The cut-off wave number is nearly the same for VPF and VCVPF for small Weber numbers and is independent of the Reynolds number.
(7) Asymptotic formulas of the dispersion relation for small and large wave numbers have been derived and the regions of applicability of these formulas evaluated. The division between large and small wave numbers is rather sharply defined by Bessel functions in the dispersion relation and is independent of the stability parameters.
(8) The differences between VPF and VCVPF are substantial when the Reynolds number is small and the Weber number is large.
(9) The relation between the symmetric mode of instability $n = 0$ and the first asymmetric mode for $n = 1$ is as in the paper by Funada et al. (2004) with $n = 1$ dominant only for small Reynolds numbers; the axisymmetric mode is always dominant for capillary instability and for Kelvin–Helmholtz instability for large Reynolds numbers.
(10) The difference between VPF and VCVPF vanishes in the inviscid limit (practically for $R > 100$) and when Kelvin–Helmholtz dominates (small W). When capillary instability dominates, the differences in the normalized growth rate discrepancy is nearly 1/2.
(11) An exact viscous solution of a two fluid problem does not allow a velocity discontinuity. However, the exact solution for pure capillary instability is very close to VCVPF which we also recommend for this more general problem.

References

Funada, T., Joseph, D.D., 2001. Viscous potential flow analysis of Kelvin–Helmholtz instability in a channel. J. Fluid Mech. 445, 263–283.

Funada, T., Joseph, D.D., 2002. Viscous potential flow analysis of capillary instability. Int. J. Multiphase Flow 28, 1459–1478.

Funada, T., Joseph, D.D., Yamashita, S., 2004. Stability of a liquid jet into incompressible gases and liquids. Int. J. Multiphase Flow 30, 1279–1310.

Joseph, D.D., Wang, J., 2004. The dissipation approximation and viscous potential flow. J. Fluid Mech. 505, 365.

Lamb, H., 1932. Hydrodynamics, sixth ed. Cambridge University Press (Reprinted by Dover, 1945).

Levich, V.G., 1949. The motion of bubbles at high Reynolds numbers. Zh. Eksperim. Tear. Fiz. 19, 18.

Wang, J., Joseph, D.D., Funada, T., 2005a. Pressure corrections for potential flow analysis of capillary instability of viscous fluids. J. Fluid Mech. 522, 383–394.

Wang, J., Joseph, D.D., Funada, T., 2005b. Pressure corrections for potential flow analysis of capillary instability of two viscous fluids. Phys. Fluids 17, 0521051-12.